Soils and Foundations 2015;55(4):798–812

HOSTED BY

ELSEVIER

CrossMark

The Japanese Geotechnical Society

Soils and Foundations

www.sciencedirect.com
journal homepage: www.elsevier.com/locate/sandf

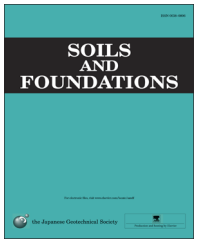

Reliability-based serviceability limit state design for immediate settlement of spread footings on clay

Jonathan C. Huffman[a], Andrew W. Strahler[b], Armin W. Stuedlein[c,*]

[a]Foundation Engineering, Inc., 820 NW Cornell Avenue, Corvallis, OR 97330, United States
[b]Oregon State University, 101 Kearney Hall, Corvallis, OR 97331, United States
[c]School of Civil and Construction Engineering, Oregon State University, 101 Kearney Hall, Corvallis, OR 97331, United States

Received 2 October 2014; received in revised form 15 February 2015; accepted 16 March 2015
Available online 1 August 2015

Abstract

While many spread footings constructed on clayey soils are designed using consolidation settlement analyses for the serviceability limit state (SLS), immediate settlement, or undrained displacement, of the footing may also contribute a significant portion of the total and/or differential settlement. Owing to possible magnitudes in immediate settlement, and with regard to stress history, assessment of the contribution of immediate settlement comprises an essential task for the understanding of the performance of a foundation system. This study proposes a simple reliability-based design (RBD) procedure for assessing the allowable immediate displacement of a spread footing supported on clay in consideration of a desired serviceability limit state. A relationship between the traditional spread footing bearing capacity equation and slope tangent capacity is established, then incorporated into a bivariate normalized bearing pressure–displacement model to estimate the mobilized resistance associated with a given displacement. The model was calibrated using a high quality database of full-scale loading tests compiled from various sources. The loading test data was used to characterize the uncertainty associated with the model and incorporated into an appropriate reliability-based performance function. Monte Carlo simulations were then used to calibrate a resistance factor with consideration of the uncertainty in the bearing pressure–displacement model, bearing capacity, applied bearing pressure, allowable displacement, and footing width. An example is provided to illustrate the application of the proposed procedure to estimate the bearing pressure for an allowable immediate displacement of a footing at the targeted probability and serviceability limit state.

Keywords: Bearing capacity; Distortion settlement; Immediate settlement; Reliability; Serviceability; Limit state design

1. Introduction

Geotechnical limit state design for spread footings requires the estimation of the bearing capacity, or the resistance at the ultimate limit state (ULS), while limiting excessive displacement to meet serviceability limit state (SLS) requirements. Bearing capacity models (e.g., Terzaghi, 1943; Hansen, 1970; Vesic, 1973, among others) for the ULS are well established for a range of soil types, and generally requires the selection or development of a limited number of design variables. The analysis for the SLS is more complicated since footing displacements consist of one or more components, including initial or immediate settlement (i.e., distortion or undrained displacement), consolidation, and secondary compression (D'Appolonia and Lambe, 1970). The contribution from each component depends on various factors such as the soil plasticity, the hydraulic conductivity, and loading rates, geometries, and magnitudes.

*Corresponding author.
E-mail address: armin.stuedlein@oregonstate.edu (A.W. Stuedlein).
Peer review under responsibility of The Japanese Geotechnical Society.

http://dx.doi.org/10.1016/j.sandf.2015.06.012

It is common for practicing engineers to focus on the consolidation component of settlement with SLS design for spread footings resting on plastic, fine-grained soils since it often provides the largest portion of the total settlement. However, immediate settlement should also be considered a critical design component for footings on plastic soils as it may comprise a significant portion of the total settlement and is essential to understanding the overall displacement behavior and undrained stability of the foundation (D'Appolonia and Lambe, 1970; D'Appolonia et al., 1971; Foye et al. 2008). Consideration of short-term construction or rapidly applied loads (e.g., live loads or seismic loads) that act quickly relative to the hydraulic conductivity of the soil are of particular concern.

Immediate settlement is the expression of shear strains that develop below and adjacent to a loaded shallow foundation and is associated with the mobilization of the shear strength of the soil (e.g., Lambe and Whitman, 1969; D'Appolonia et al., 1971). Unlike primary consolidation and secondary compression, there is significant uncertainty associated with available analytical methods for use with plastic fine-grained soils (Strahler and Stuedlein, 2013). Although accepted immediate settlement models often assume an elastic soil response (e.g., AASHTO, 2012, Eurocode 7 Orr and Breysse, 2008), the stress–strain characteristics of soils follow a nonlinear path at relatively small footing displacements (e.g., D'Appolonia et al., 1971; Jardine et al., 1986; Foye et al., 2008; Stuedlein and Holtz, 2010; Strahler and Stuedlein, 2013). The nonlinear behavior must be incorporated into an appropriate analytical model to predict the footing response.

Separately, the uncertainty associated with an appropriate analytical model must be characterized if the transition to a reliability-based limit state design and harmonization with existing design codes will be achieved. This requires that the multiple sources of uncertainty associated with the SLS be characterized including model uncertainty (e.g., Phoon, 2003, 2008; Li et al., 2013; Uzielli and Mayne, 2011; Wang, 2011; Huffman and Stuedlein, 2014), and incorporate the uncertainty within a probabilistic framework to estimate the displacement of footings with a pre-determined reliability. Fenton et al. (2005) present a reliability approach for immediate settlements in consideration of spatial variability using the random finite element method and linear elastic constitutive laws, and Wang (2011) presented an expanded RBD approach for spread foundations that considers cost-optimization. The benefit of the approach by Fenton et al. (2005) is that the autocorrelation distance and inherent variability of the elastic stiffness may be incorporated directly; however, the true nonlinear behavior of foundations undergoing distortion settlement is not captured by either Fenton et al. (2005) or Wang (2011), which could result in significant error for heavily loaded foundations in plastic fine-grained soils. Roberts and Misra (2010) present an SLS design methodology for spread footings, but this approach was limited to elastic–plastic bearing pressure–displacement response.

Huffman and Stuedlein (2014) described a reliability-based SLS procedure for shallow foundations resting on aggregate pier (or stone column) reinforced clayey soils that accounted for soil nonlinearity. However, such a framework does not presently exist for unreinforced plastic, fine-grained soils. To address the potential shortcomings in available methods for the estimation of immediate settlement for serviceability design of shallow foundations bearing on saturated, plastic fine-grained soils, this study uses the results from 30 full-scale loading tests on unreinforced clayey subgrades and a selected bearing capacity (ULS) model to develop a novel reliability-based SLS design procedure for nonlinear, inelastic immediate settlement. First, the loading test database compiled by Strahler (2012) and characterized by Strahler and Stuedlein (2014) is described, and the capacity inferred from each loading test, $q_{ult,i}$, is compared to the capacity calculated using a traditional bearing capacity model, $q_{ult,p}$, to estimate the model bias and uncertainty associated with the ULS. A relationship between the ULS and a new reference capacity is then established to reduce the dispersion of the bearing pressure–displacement (q–δ) response. Bivariate hyperbolic and power law models are then investigated for possible use for simulating the normalized q–δ response over a range of typical bearing pressures and displacements. Owing to the multi-dimensional correlation between the normalized q–δ parameters representing the hyperbolic model and the selected reference capacity, a computationally efficient vine copula approach is implemented in the reliability simulations. To improve the estimate of SLS reliability, a suitable lower bound ULS capacity to limit unreasonably low values of capacity is imposed by considering the remolded shear strength of typical fine-grained soils. Monte Carlo simulations (MCS) are then used to formulate a procedure to generate the calibrated, lumped load-and-resistance factor used to estimate the bearing pressure associated with a given displacement and its probability of exceedance. The MCS accounts for the uncertainty in the ULS capacity, normalized q–δ model, applied bearing pressure, allowable displacement, and footing width. The new procedure developed herein is appropriate for the reliability-based assessment of nonlinear, inelastic immediate settlement resulting from rapid loading of rigid footings on saturated, plastic fine-grained soils.

2. Load test database and ULS bearing capacity model

Reliability analyses using a high quality loading test database allows the assessment of design model bias and uncertainty across a range of differing geologic conditions, construction techniques, and other relevant design variables (Stuedlein et al., 2012). The new and original database compiled by Strahler (2012) and Strahler and Stuedlein (2014) included 30 loading tests of various-sized spread footings supported on soft to very stiff, plastic, fine-grained soil at 12 different sites located throughout Asia, Europe and North America. The criteria for the selection of cases for the database included: (1) a relatively uniform soil profile to at least $2B$ below the base of the footing (where B is the footing width or diameter) consisting of plastic, fine-grained soil acting in an undrained manner during loading, (2) adequate in-situ and/or laboratory data to determine representative soil conditions (e.g., undrained shear strength, s_u), (3) sufficient description of the load test setup and loading protocol, (4) footing embedment depth less than $4B$ to ensure a shallow failure mechanism, (5) a rigid footing response, and (6) sufficient

Table 1
Summary of load test database.

Source	Test	Footing shape	B (m)[a]	B' (m)[b]	D_f (m)[c]	D_w (m)[d]	s_u (kPa)[e]	γ_m (kN/m^3)[f]
Andersen and Stenhamar (1982)	HA-1	Square	1.00	1.13	0.0	10.0	48	22.0
	HA-2	Square	1.00	1.13	0.0	10.0	48	22.0
Bauer et al. (1976)	OB-1	Circle	0.46	0.46	2.60	1.75	74	17.9
	OB-2	Square	3.10	3.50	0.66	1.75	108	17.9
Bergado et al. (1984)	RB-1	Circle	0.30	0.30	0.0	1.00	37	14.9
Brand et al. (1972)	BB-1	Square	1.05	1.18	1.60	0.90	20	19.5
	BB-2	Square	0.90	1.02	1.60	0.90	20	19.5
	BB-3	Square	0.75	0.85	1.60	0.90	20	19.5
	BB-4	Square	0.67	0.76	1.60	0.90	21	19.5
	BB-5	Square	0.60	0.68	1.60	0.90	21	19.5
Deshmukh and Ganpule (1994)	BD-1	Square	0.60	0.68	0.60	0.60	20	17.7
	BD-2	Square	0.60	0.68	0.60	0.60	20	17.7
Greenwood (1975)	GG-1	Square	0.91	1.03	0.61	>10.0	44	18.5
Jardine et al. (1995)	BH-1	Square	2.20	2.48	0.78	0.90	21	16.0
Lehane (2003)	BL-1	Square	2.00	2.26	1.60	1.40	20	17.0
Marsland and Powell (1980)	CM-1	Circle	0.87	0.87	0.0	>10.0	139	19.5
Newton (1975)	ON-1	Circle	0.60	0.60	0.38	0.31	20	18.5
	ON-2	Circle	0.49	0.49	0.38	0.31	20	18.5
	ON-3	Circle	0.34	0.34	0.38	0.31	20	18.5
Stuedlein and Holtz (2010)	TS-1	Circle	0.76	0.76	0.61	2.40	70	19.7
	TS-2	Circle	0.76	0.76	0.61	2.40	70	19.7
	TS-3	Square	2.74	3.09	0.0	2.40	85	19.7
Tand et al. (1986)	TT-1	Circle	0.58	0.58	1.50	0.90	44	20.0
	TT-2	Circle	0.58	0.58	1.50	0.90	44	20.0
	TT-3	Circle	0.58	0.58	1.50	0.90	44	20.0
	TT-4	Circle	0.58	0.58	1.50	0.90	45	20.0
	TT-5	Circle	0.58	0.58	1.50	0.90	45	20.0
	TT-6	Circle	0.58	0.58	1.50	1.10	67	20.0
	TT-7	Circle	0.58	0.58	1.50	1.10	67	20.0
	TT-8	Circle	0.58	0.58	1.50	1.10	67	20.0

[a]Footing width or diameter.
[b]Equivalent footing width.
[c]Footing embedment depth.
[d]Ground water depth.
[e]Soil undrained shear strength.
[f]Soil unit weight.

footing displacement to estimate the non-linear response of the soil (Strahler and Stuedlein, 2014). The new load test database is summarized in Table 1.

Importantly, the database assembled for this study consisted of footing loading tests with various kinds of instrumentation, and not all case histories were characterized with sufficient instrumentation to confirm that the subgrade acted in an undrained manner. However, several well-instrumented loading tests provided evidence of undrained displacements and were used as a basis for comparison of cases and evaluation of admissibility to the database. For example, the pore pressure response exhibited by the saturated, medium stiff clay subgrade (s_u=48 kPa) reported by Andersen and Stenhamar (1982) and saturated, soft clay subgrade (s_u=21 kPa) reported by Jardine et al. (1995) indicated undrained responses. Stuedlein and Holtz (2010) compared the vertical and lateral displacements measured to the theoretical displacements assuming zero volume change, and showed that an undrained response was achieved at large displacements (Stuedlein and Holtz, 2010). Such responses are anticipated for footing loading tests conducted rapidly in plastic, fine-grained deposits owing to their low hydraulic conductivities and coefficients of consolidation. The database did not include those high quality case histories with layered soil conditions (e.g., Consoli et al., 1998), with possible drainage paths within 2B of the footing base. Additionally, each test admitted to the database was conducted over a period of minutes or hours, rather than months. Thus, the footing subgrades admitted into the loading test database may be assumed to respond in a relatively undrained manner, and are representative of typical immediate settlement scenarios.

Bearing pressure–displacement (q–δ) data were compiled from the individual tests and the ultimate resistance (i.e., bearing capacity) was determined by extrapolation of the q–δ data using fitted hyperbolic curves. The interpreted capacity, $q_{ult,i}$, was set equal to the estimated asymptote resulting from the fitted hyperbolic relationship. A predicted capacity, $q_{ult,p}$, was calculated for each test using the general bearing capacity equation (e.g., Terzaghi, 1943) with Meyerhof (1963) bearing capacity factors, and shape and depth factors proposed by Hansen (1970). Assuming undrained loading conditions, the bearing capacity equation for a general shear failure for the

footings in the database considered equals:

$$q_{ult,p} = s_u N_c \lambda_{cs} \lambda_{cd} + \gamma D_f N_q \lambda_{qs} \lambda_{qd} \quad (1)$$

where s_u is the undrained shear strength, γ is the unit weight, D_f is the footing embedment depth, N_c and N_q represent bearing capacity factors (assumed equal to 5.14 and 1.0, respectively, for the $\phi=0$ condition), and λ_{cs}, λ_{qs}, λ_{cd} and λ_{qd} are Hansen (1970) shape and depth factors, respectively. The factors λ_{qs} and λ_{qd} were assumed to be 1.0 for $\phi=0$ soil, and shape factors were computed in accordance with the relevant geometry (i.e., circular or square). The interpreted and predicted bearing capacities for each loading test are summarized in Table 2. The bias for each test, defined as the ratio of the interpreted and predicted bearing capacity, is also summarized Table 2. The mean bias was equal to $M_{ult}=1.25$, indicating Eq. (1) underpredicted the interpreted capacity by 25 percent on average. The coefficient of variation (COV) in bias was equal to 37 percent, indicating moderate-to significant variability. The capacity model error is typical in geotechnical applications, and underscores the need to appropriately characterize model uncertainty for reliability-based limit state design.

3. Bearing pressure–displacement model

Serviceability limit state design of spread footings is controlled by the allowable displacement. The undrained loading of plastic fine-grained soils follow a nonlinear path even at relatively small foundation displacements. Akbas and Kulhawy (2009) and Uzielli and Mayne (2011), among others, showed that nonlinear q–δ behavior for spread footings, with applied pressure normalized by a reference capacity or in-situ measurement, q_{ref}, respectively, and displacement normalized by footing size, can be represented using a hyperbolic model:

$$q* = \frac{q_{mob}}{q_{ref}} = \frac{\eta}{k_1 + k_2 \cdot \eta} \quad (2)$$

or power law:

$$q* = \frac{q_{mob}}{q_{ref}} = k_3 \cdot \eta^{k_4} \quad (3)$$

respectively, where q_{mob} is the mobilized resistance at a given displacement, δ, $\eta=\delta/B'$ is the normalized displacement, and B' is the equivalent footing diameter, defined as the diameter that produces the same area as that of a square footing (e.g., Mayne and Poulos, 1999).

Table 2
Comparison of interpreted, calculated, and slope tangent capacities with corresponding ratios.

Test	Interpreted capacity, $q_{ult,i}$ (kPa)	Calculated capacity, $q_{ult,p}$ (kPa)	Bias $q_{ult,i}/q_{ult,p}$	Slope tangent capacity, q_{STC} (kPa)	$q_{STC}/q_{ult,i}$
HA-1	343	298	1.15	342	1.00
HA-2	378	298	1.27	–	–
OB-1	560	746	0.75	305	0.54
OB-2	515	735	0.70	–	–
RB-1	180	231	0.78	125	0.69
BB-1	177	191	0.93	–	–
BB-2	213	196	1.09	171	0.80
BB-3	228	204	1.12	177	0.78
BB-4	227	209	1.09	–	–
BB-5	271	211	1.28	–	–
BD-1	262	175	1.50	–	–
BD-2	365	175	2.09	–	–
GG-1	313	347	0.90	217	0.69
BH-1	205	160	1.28	118	0.58
BL-1	120	186	0.64	91	0.76
CM-1	539	858	0.63	–	–
ON-1	415	162	2.56	187	0.45
ON-2	221	169	1.31	125	0.57
ON-3	342	172	1.99	–	–
TS-1	754	582	1.29	477	0.63
TS-2	774	582	1.33	458	0.59
TS-3	568	527	1.08	384	0.68
TT-1	750	429	1.75	426	0.57
TT-2	734	429	1.71	414	0.56
TT-3	684	429	1.59	443	0.65
TT-4	382	436	0.88	176	0.46
TT-5	225	436	0.52	158	0.70
TT-6	1021	640	1.59	607	0.59
TT-7	963	640	1.50	599	0.62
TT-8	844	640	1.32	494	0.59
			Mean = 1.25		**Mean = 0.643**
			COV = 0.367		**COV = 0.187**

Note: Values of q_{STC} are reported only for load tests taken to a footing displacement of at least $0.03B'$.

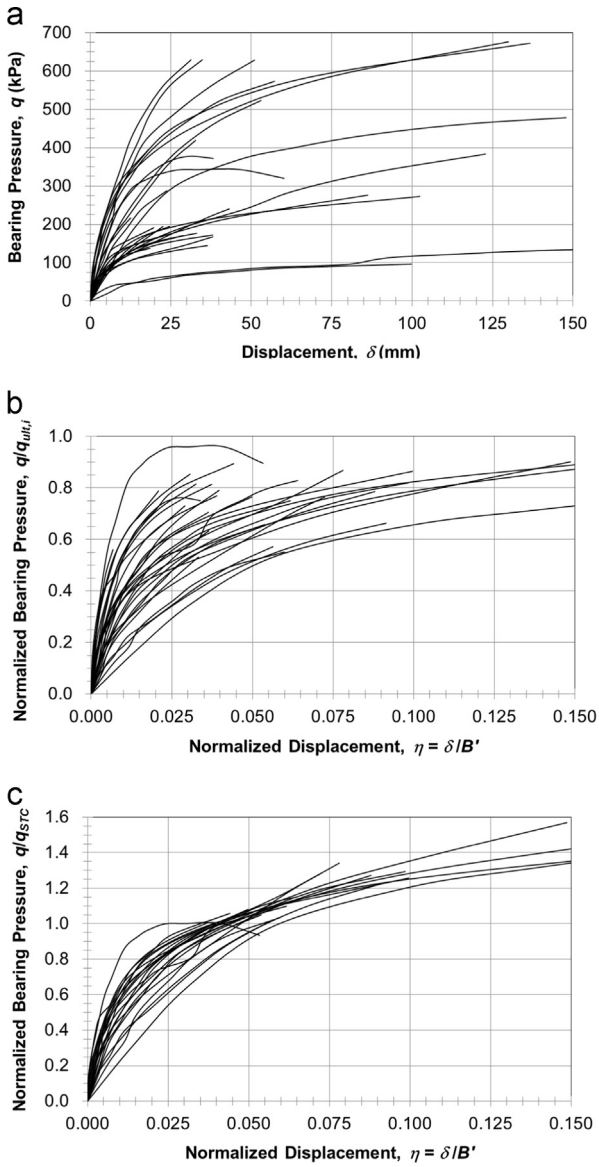

Fig. 1. Variation of bearing pressure with displacement for footings in the load test database: (a) observed q–δ response, (b) normalized q–δ response using $q_{ult,i}$ and (c) normalized q–δ response using q_{STC}.

Table 3
Summary of bearing pressure–displacement model coefficients and goodness-of-fit parameters.

	Hyperbolic model					Power law model				
Test	k_1	k_2	RMSE	R^2	Mean bias	k_3	k_4	RMSE	R^2	Mean bias
HA-1	0.003	0.958	20.49	0.97	1.00	2.68	0.29	37.68	0.83	0.95
HA-2	0.007	0.763	12.02	0.99	1.00	4.69	0.43	28.17	0.91	0.97
OB-1	0.030	0.544	7.86	1.00	0.99	2.51	0.36	30.91	0.93	0.98
OB-2	0.005	0.851	3.57	1.00	0.93	14.11	0.62	6.78	0.99	0.98
RB-1	0.013	0.682	2.03	1.00	0.98	4.62	0.49	7.88	0.93	0.96
BB-1	0.005	0.855	2.59	1.00	1.04	4.42	0.41	5.97	0.96	0.96
BB-2	0.007	0.808	1.19	1.00	1.01	4.60	0.44	8.48	0.95	0.96
BB-3	0.009	0.771	0.97	1.00	1.00	4.83	0.47	8.28	0.96	0.97
BB-4	0.007	0.822	3.00	1.00	1.01	4.49	0.43	5.78	0.97	0.98
BB-5	0.011	0.730	1.88	1.00	0.98	5.93	0.53	9.58	0.94	0.96
BD-1	0.008	0.783	3.56	1.00	1.01	5.61	0.50	10.26	0.96	0.95
BD-2	0.019	0.614	4.23	0.99	0.99	8.77	0.68	5.05	0.89	0.98
GG-1	0.011	0.688	5.62	1.00	0.98	3.24	0.39	19.38	0.93	0.96
BH-1	0.012	0.721	5.54	0.98	1.02	4.04	0.45	4.00	0.98	0.99
BL-1	0.006	0.845	5.38	0.97	1.10	3.53	0.37	2.81	0.96	0.98
CM-1	0.005	0.852	10.25	0.99	1.01	4.99	0.43	8.65	0.99	0.99
ON-1	0.017	0.596	11.40	0.98	1.11	4.98	0.52	2.69	1.00	1.00
ON-2	0.011	0.647	9.83	0.98	1.39	3.70	0.40	2.53	0.99	1.00
ON-3	0.014	0.652	3.71	1.00	1.04	6.75	0.58	4.95	0.99	0.98
TS-1	0.011	0.658	27.03	0.99	1.07	2.57	0.32	31.01	0.93	0.97
TS-2	0.013	0.614	39.21	0.98	1.27	2.74	0.33	18.94	0.95	0.97
TS-3	0.010	0.792	17.76	0.98	1.17	4.84	0.49	4.16	1.00	0.99
TT-1	0.025	0.540	7.54	1.00	1.04	4.94	0.56	14.30	0.99	0.96
TT-2	0.025	0.565	10.01	0.99	1.06	6.31	0.63	5.26	0.99	0.99
TT-3	0.015	0.634	12.07	1.00	1.05	3.90	0.45	21.88	0.97	0.95
TT-4	0.014	0.574	16.15	0.96	1.05	3.07	0.35	3.73	0.98	1.00
TT-5	0.011	0.707	4.95	0.99	1.01	4.44	0.46	8.76	0.96	0.98
TT-6	0.024	0.532	14.41	0.99	0.98	6.69	0.64	30.25	0.90	0.95
TT-7	0.017	0.627	4.90	1.00	1.00	5.86	0.57	23.54	0.97	0.96
TT-8	0.016	0.618	11.97	1.00	1.03	4.28	0.48	20.45	0.98	0.97
Mean	**0.013**	**0.701**	**9.37**	**0.99**	**1.04**	**4.94**	**0.47**	**13.07**	**0.96**	**0.97**

The reference capacity, q_{ref}, is used as a means to both normalize the resistance and reduce scatter inherent with load test data. The reference capacity does not necessarily represent a true "capacity", rather, it should provide a replicable means to produce a known capacity, and preferably linked to a predetermined deflection criterion. For example, Akbas and Kulhawy (2009) used the failure load interpreted from load tests to represent q_{ref}, whereas Uzielli and Mayne (2011) used the cone tip resistance to represent q_{ref}. For this study, both the interpreted capacity, $q_{ult,i}$, and slope tangent capacity, q_{STC} (e.g., Phoon and Kulhawy, 2008), were investigated for potential use as a reference capacity. The slope tangent capacity with a displacement offset equal to $0.03B'$ was ultimately selected to represent the reference capacity because it significantly reduced the dispersion of the q^*–η curves compared to the interpreted capacity, $q_{ult,i}$, it could be readily estimated as a function of $q_{ult,i}$, and it is linked to a well-characterized magnitude of displacement. Fig. 1 shows the bearing pressure–displacement curves for all footings in the load test database (Fig. 1a) along with the normalized (i.e., q^*–η) curves, where q^* was established using $q_{ref}=q_{ult,i}$ (Fig. 1b) and $q_{ref}=q_{STC}$ (Fig. 1c). The scatter in the q^*–η curves associated with q_{STC} (Fig. 1c) is significantly reduced in comparison to the other bearing pressure–displacement curves, providing a more suitable approach for simulating continuous nonlinear q^*–η behavior in the reliability analyses, described below.

The coefficients k_1, k_2, k_3 and k_4 in Eqs. (2) and (3) were determined using linear least squares optimization and allow the simulation of continuous q^*–η curves. The best-fit coefficients for each loading test are summarized in Table 3. In nine of the 30 cases where the loading test was not taken to a displacement of at least $0.03B'$, the fitting coefficients were determined with a q_{STC} value estimated by extrapolating the nonlinear bearing pressure–displacement response. Although the results suggest that both the hyperbolic and power law models can be used to accurately predict immediate undrained

displacement, goodness-of-fit measures including the sum of the root mean square error (RMSE), coefficient of determination (R^2), and mean bias indicate that the hyperbolic model produced a slightly better overall fit to the q^*–η behavior. Therefore, the hyperbolic model (Eq. (2)) was selected for use in the subsequent reliability calibrations.

The reference capacity, q_{STC}, used with the bearing pressure–displacement model is specific to a given footing loading test. Thus q_{STC} must be estimated for the typical case where a site-specific loading test has not been performed. Fig. 2 shows that a linear relationship between q_{STC} and $q_{ult,i}$ exists, suggesting that q_{STC} can be readily estimated as a function of the interpreted capacity; a similar correlation was noted in separate SLS simulations reported by Stuedlein and Uzielli (2014). The ratios of q_{STC} to $q_{ult,i}$ for the loading tests are summarized in Table 2, and exhibit a mean ratio of 0.643. In turn, $q_{ult,i}$ must also be estimated in the absence of site-specific loading tests, which is accomplished using the bearing capacity equation (Eq. (1)). The mobilized resistance may be estimated as a function of displacement using the predicted bearing capacity, $q_{ult,p}$:

$$q_{mob} = \frac{\eta}{k_1 + k_2\eta} q_{STC} = \frac{\eta}{k_1 + k_2\eta} M_{STC} q_{ult,p} = M_\eta M_{STC} q_{ult,p} \tag{4}$$

where $q_{ult,p}$ is calculated from Eq. (1), M_{STC} is the model factor used to scale the predicted ultimate resistance to the slope tangent resistance and equals the mean of $q_{STC}/q_{ult,i}$ (i.e., 0.643, see Fig. 2), and M_η is the hyperbolic model factor used to scale to the mobilized resistance based on the allowable normalized undrained footing displacement, η. In order to ensure that the reliability-based SLS calibrations are accurate, the model uncertainty associated with the bearing capacity estimate $q_{ult,p}$ (Eq. (1)), as well as the uncertainty associated with the normalized bearing pressure–displacement model (Eq. (2)), and the parameters k_1 and k_2, and q_{STC} must be incorporated in a systematic basis. The framework used to accomplish this is described in the following section.

4. Application of bearing pressure–displacement model to reliability-based design

Reliability-based limit state design requires calibration of appropriate load and resistance factors that are based on the uncertainty associated with the design input parameters. Input parameters associated with estimating the serviceability-level resistance for spread footings on clay were described previously (i.e., $q_{ult,p}$, M_{STC}, k_1 and k_2). Additional sources of uncertainty include the load and structural response parameters, such as the design bearing pressure, the allowable settlement, and footing size.

Incorporating this uncertainty into the limit state design may be efficiently accomplished using probabilistic methods and an appropriate performance function, P. The margin of safety, defined as the difference between the resistance, R, and load, Q, represents an appropriate performance function with a corresponding joint probability distribution function. In consideration

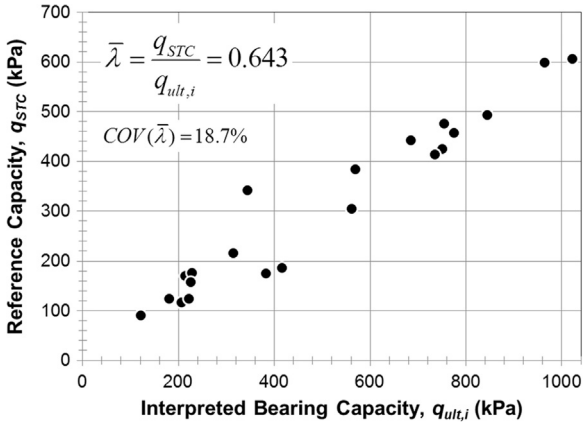

Fig. 2. Variation of the reference slope tangent capacity with the interpreted bearing capacity.

of the various sources of uncertainty contributing to the system reliability, the probability of failure, p_f, may be defined using the margin of safety and represented by Baecher and Christian (2003), Allen et al. (2005), Phoon (2008):

$$p_f = Pr(R - Q < 0) = Pr(P < 0) \le p_T \tag{5}$$

where p_T is the acceptable target probability that the load will be greater than the resistance, typically in the range of 1 to 0.1 percent for geotechnical ultimate limit state applications and 20 to 1 percent for geotechnical serviceability limit state applications. The performance function may be reformulated in terms of the allowable mobilized bearing resistance, q_{mob}, and an applied bearing pressure, q_{app}, by incorporating the selected bearing pressure–displacement model (Eq. (4)):

$$p_f = Pr(M_{STC} M_\eta q_{ult,p} - q_{app} < 0) = Pr\left(M_{STC} M_\eta < \frac{q_{app}}{q_{ult,p}}\right) \le p_T \tag{6}$$

The characteristic distributions of each random variable can be incorporated into the performance function by defining the ultimate and applied bearing pressures in terms of a deterministic nominal value (i.e., $q_{app,n}$ and $q_{ult,n}$) and the corresponding normalized random variables (i.e., q^*_{app} and q^*_{ult}), with Eq. (6) rewritten as (Uzielli and Mayne, 2011)

$$p_f = Pr\left(M_{STC} M_\eta < \frac{q_{app,n} \cdot q^*_{app}}{q_{ult,n} \cdot q^*_{ult}}\right) = Pr\left(M_{STC} M_\eta < \frac{1}{\psi_q} \frac{q^*_{app}}{q^*_{ult}}\right) \le p_T \tag{7}$$

where ψ_q is the combined (i.e., lumped) load and resistance factor assigned to provide an acceptable probability of failure. The lumped load and resistance factor is preferred to partial factors as current design codes (e.g., AASHTO, 2012 or Eurocode 7) recommend partial factors equal to 1.0 for SLS design of spread footings without the consideration of uncertainty.

For this study, p_f, and the associated reliability index, $\beta = -\Phi^{-1}(p_f)$, where Φ^{-1} represents the inverse standard normal cumulative function, were estimated based on a prescribed interval of ψ_q that ranged from one (i.e., no reduction in

applied bearing pressure) to 20, and determined using Monte Carlo simulations (MCS) seeded with distributions for each of the varied parameters. The results of the simulations were used to investigate possible relationships between the parameters in the performance function and to provide a simplified procedure for SLS design.

5. Simulation-based serviceability limit state design calibrations

To calibrate the lumped load and resistance factor using an appropriate performance function distribution, the MCS incorporated uncertainty in the bearing capacity model, the normalized bearing pressure–displacement model, the relationship between slope tangent and ultimate bearing capacities, the allowable displacement, the footing width, and the applied loading. Tables 4 and 5 summarize the statistical parameters of all of the random variables in the reliability simulations. Selection of the nominal values and model distribution of the load and resistance variables are discussed below.

6. Characterization of resistance parameters

The nominal values and characteristic distributions for the resistance variables were estimated from the loading test database and normalized bearing pressure–displacement model as follows:

- The nominal bearing capacity, q^*_{ult}, was set equal to the mean bias between the calculated and interpreted capacities ($q_{ult,p}$ and $q_{ult,i}$, respectively), from the loading test database, and the distribution estimated by fitting to the sample biases summarized in Table 2.
- The nominal slope tangent capacity scaling factor, M_{STC}, was set equal to the mean ratio of $q_{ult,i}$ to q_{STC}, and the distribution estimated by fitting to the sample ratios summarized in Table 2.
- The nominal value of the hyperbolic model parameters, k_1 and k_2, were estimated as the mean k_1 and k_2 values indicated in Table 3, and distributions were estimated by fitting to the sample values in Table 3.

The selected model distributions resulted from fitting to several possible distributions and evaluated using the Akaike Information Criteria (*AIC*; Akaike, 1974) and Bayesian Information Criterion (*BIC*; Schwarz, 1978) goodness-of-fit tests. The *AIC* and *BIC* are defined as

$$AIC = -2\sum_{i=1}^{N} \ln f_{pdf}(x_i) + 2k \tag{8}$$

$$BIC = -2\sum_{i=1}^{N} \ln f_{pdf}(x_i) + k \ln N \tag{9}$$

respectively, where f_{pdf} is the probability density function (*pdf*) of a selected distribution, N is the sample size with x_i representing a sample value from the dataset, and k is the number of parameters associated with the given *pdf*. The best-fit model distributions were selected by choosing the distribution that resulted in the lowest *AIC* and *BIC* values, shown in Table 4. The lognormal, gamma, inverse Gaussian, and beta distributions were assessed for suitability of sampling in the MCS. Normal distributions were not included to avoid the potential for negative values leading to inaccurate and/or inappropriate results in the reliability simulations. Note that because the distributions were fit to data available, their robustness should be investigated as new high quality data becomes available. The normalized resistance model parameters selected for use in the reliability simulations based on the best-fit distributions is summarized in Table 5.

Table 4
Summary of AIC and BIC values for selected distributions fit to normalized resistance model parameters (bold values represent lowest AIC and BIC).

Parameter	Distribution	AIC	BIC
q^*_{ult}	Lognormal	42.41	45.69
	Gamma	**42.08**	**45.36**
	Inverse Gaussian	42.33	45.61
	Beta (general)	44.11	48.12
M_{STC}	**Lognormal**	**−24.94**	**−23.23**
	Gamma	−19.80	−18.07
	Inverse Gaussian	−24.90	−23.18
	Beta (general)	n/a	n/a
k_1	Lognormal	−214.54	−211.26
	Gamma	**−215.05**	**−211.77**
	Inverse Gaussian	−214.71	−211.43
	Beta (general)	−212.91	−208.91
k_2	Lognormal	−41.06	−37.78
	Gamma	−41.26	−37.98
	Inverse Gaussian	**−41.85**	**−38.57**
	Beta (general)	n/a	n/a

Table 5
Summary of fitted normalized resistance model parameters.

Parameter	Mean	*COV* (%)	Model distribution
q^*_{ult}	1.25	37.3	Gamma
M_{STC}	0.643	18.7	Lognormal
k_1	0.013	53.0	Gamma
k_2	0.701	16.1	Inverse Gaussian

7. Resistance parameter dependence and Copula analyses

The potential dependence between random variables must be incorporated in reliability simulations to avoid hidden biases that may skew the resulting calibrations (e.g., Phoon and Kulhawy, 2008; Uzielli and Mayne, 2011, 2012; Stuedlein et al., 2012; Tang et al., 2013, Huffman and Stuedlein, 2014). The q^*–η model parameters (M_{STC}, k_1 and k_2) showed no apparent correlation to the bearing capacity parameters (s_u, γ' and D_f), as indicated in Fig. 3. However, each of the q^*–η

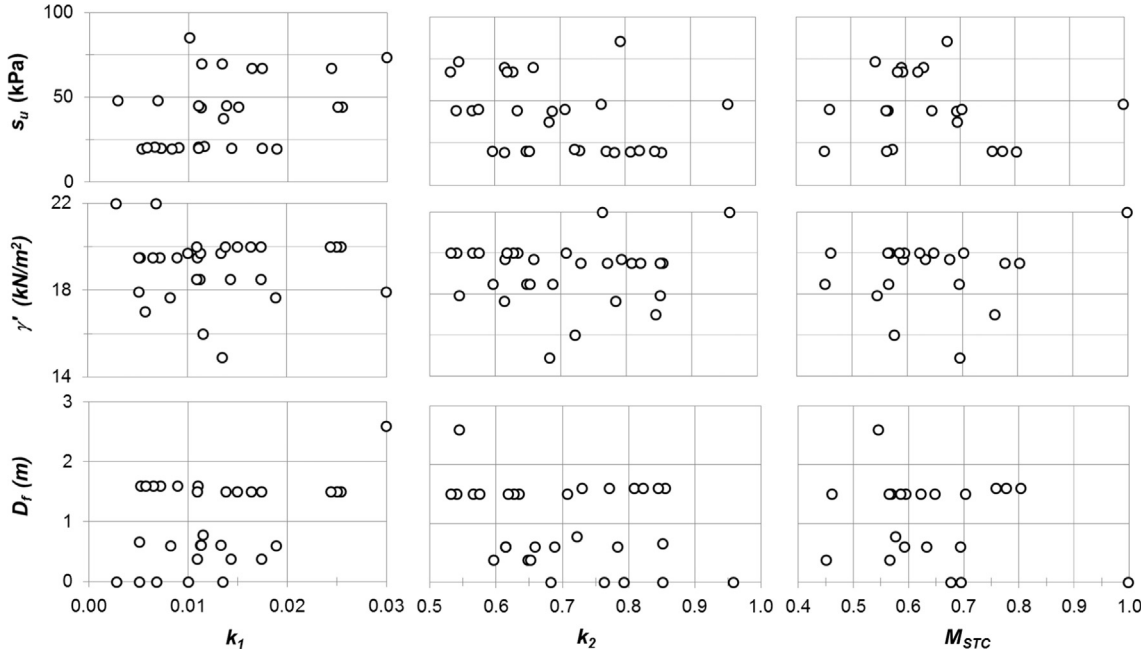

Fig. 3. Variation of normalized bearing pressure–displacement model parameters k_1 and k_2, and model factor M_{STC} with geometric and soil properties influencing bearing capacity.

model parameters showed moderate to strong correlation to each other as shown in Fig. 4. Kendal's rank tau correlations, ρ_τ, of -0.80, -0.59 and 0.62 were calculated for the k_1-k_2, k_1-M_{STC} and k_2-M_{STC} pairs, respectively. Such correlations are common for bivariate load–displacement models used in geotechnical applications (e.g., Phoon and Kulhawy, 2008; Stuedlein and Reddy, 2013; Huffman and Stuedlein, 2014).

Copula functions were used to account for the multivariate dependence (i.e., joint distribution) in the reliability simulations. A copula function describes the probability of values in a dataset, similar to the fitted distributions for the individual variables. However, instead of describing the probability distribution of a single variable, the copula function describes the probable values of one variable given the values of the other, correlated variables. These results can then be coupled with the marginal distributions of the individual variables to provide a full description of the probable values (e.g., Nelson, 2006). Bivariate copula functions have been used in other recent geotechnical-related studies to account for the dependence between load and displacement model parameters (e.g., Uzielli and Mayne, 2011, 2012; Li et al., 2013; Huffman and Stuedlein, 2014) and between soil strength parameters (e.g., Tang et al., 2013, 2015; Wu, 2013, 2015).

Many copula types are available to account for trends in correlations, including linear or nonlinear correlations, elliptical correlations, and tail-dependent correlations, among others. Most copula functions can be calibrated using a single copula parameter, θ, to define the dependence structure between variables. The copula parameter may be calculated based on a relationship to ρ_τ that is specific to the copula type.

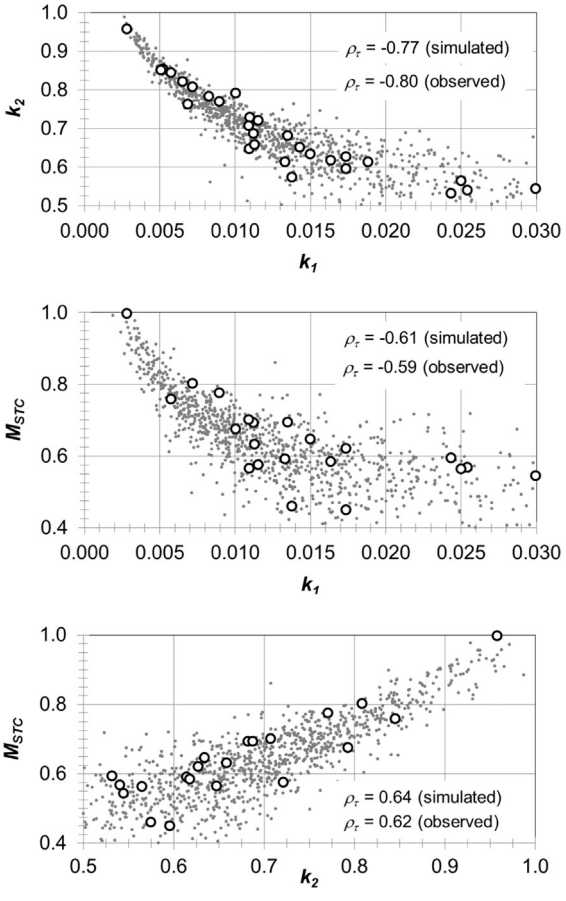

Fig. 4. Comparison of observed and simulated ($n=1000$) normalized bearing pressure–displacement model parameters k_1 and k_2, and model factor M_{STC}.

Table 6
Summary of best-fit copula functions representing bivariate dependence in the vine copula

Dependent pair	Best-fit Copula	Copula parameter, θ	Copula probability function, $C(u, v)$	General copula density function, $c(u, v)$
k_1-k_2	Clayton (rotated 270°)	−7.054	$u-\left(u^{-\theta}+(1-v)^{-\theta}-u^{-\theta}(1-v)^{-\theta}\right)^{-\frac{1}{\theta}}$	$\frac{\partial}{\partial u \partial v} C(u, v)$
k_1-M_{STC}	Clayton (rotated 270°)	−3.143	$u-\left(u^{-\theta}+(1-v)^{-\theta}-u^{-\theta}(1-v)^{-\theta}\right)^{-\frac{1}{\theta}}$	
k_2–M_{STC}	Joe (rotated 180°)	1.398	$u+v-1-\left(1-\left((1-u)^{-\theta}+(1-v)^{-\theta}-1\right)^{\frac{1}{\theta}}\right)$	

Note: Coefficients u and v represent the rank values of the dependent pairs transposed to [0,1] space (e.g., u_1 and u_2 for the k_1-k_2 pairs).

Copula functions assume uniformly distributed marginal distributions in rank [0,1] space. Therefore, the rank values of the hyperbolic model parameters and model factor (k_1, k_2 and M_{STC}), referred to herein as u_1, u_2 and u_{STC}, were used with ρ_τ to establish θ and the copula probability function. A relationship between two variables (e.g., k_1 and k_2) and a two-parameter copula probability function, $C_{k1,k2}$, is determined by fitting to ρ_τ using (e.g., Nelson, 2006; Li et al., 2013):

$$\rho_\tau(k_1,k_2)=4\int_0^1\int_0^1 C_{k_1,k_2}(u_1,u_2)dC_{k_1,k_2}(u_1,u_2)-1 \quad (10)$$

Dependence between three or more variables can be accounted for using one multivariate copula, or a string of bivariate copulas, known as a vine copula (e.g., Joe, 1996; Aas et al., 2009; Brechmann and Schepsmeier, 2013). The vine copula approach was selected to represent the dependence between k_1, k_2 and M_{STC} because it is not limited to a single dependence structure and therefore may provide better representation of the correlation between individual variables relative to a single multivariate copula (Brechmann and Schepsmeier, 2013). The selection of the bivariate copulas included in the vine, as well as selection of the copula parameters, θ, required multiple iterations to determine the best-fit copulas. A canonical (i.e., C-vine) approach (Aas et al., 2009; Brechmann and Schepsmeier, 2013) was selected for the simulations herein, which establishes the best-fit bivariate copulas using sequential maximum likelihood estimation (e.g., Lipster and Shiryaev, 2001). The order of the variables for this analysis was arbitrarily taken as: (1) k_1, (2) k_2, and (3) M_{STC}, because initial studies showed that the reliability simulations were not sensitive to the order of simulation.

The best-fit copulas were selected from several copula types based on the AIC criteria similar to that used for the marginal distributions (i.e., Eq. (8)). For each set of dependent variables (i.e., k_1-k_2, k_1-M_{STC} and k_2-M_{STC},), the AIC test was used to estimate the relative likelihood of a two-parameter copula density function, c. Based on these test criteria, the multi-dimensional vine copula was constructed using the bivariate Clayton copula (rotated 270 degrees) to represent the dependence between k_1-k_2 and k_1-M_{STC}, and the bivariate Joe copula (rotated 180 degrees) was selected to represent the dependence of k_2-M_{STC}. A summary of the selected copula types with the respective copula probability functions and θ values is shown in Table 6. Fig. 4 shows the fitted k_1-k_2, k_1-M_{STC} and k_2-M_{STC} pairs from the load test database compared against 1000 simulated pairs using the distributions indicated in Table 5 and variable dependence with vine copula components indicated in Table 6. The ρ_τ values for the actual and simulated data pairs shown in Fig. 4 indicate close agreement between observed and simulated data pairs, and indicate that the simulated values adequately represent the distribution and dependence of the q^*–η model parameters extrapolated from the load test database.

8. Assessment of lower-bound resistance

Najjar and Gilbert (2009) describe the impact of physically meaningful lower-bound soil strength on the reliability of geotechnical performance of driven pile foundations. The lower-bound soil strength is best determined using site-specific soil investigations, with particular attention to stress history, mineralogy, and secondary soil structure. Najjar (2005) suggests that the lower-bound capacities for foundations on fine-grained soils is limited by the remolded undrained shear strength, s_{ur}. Therefore, to estimate and characterize the lower-bound capacity reflected in the database considered herein, the bearing capacity was recalculated for each case history using the general bearing capacity equation (Eq. (1)) with s_{ur} instead of s_u. Residual shear strength with depth measurements were report by Bauer et al. (1976), and soil sensitivity (s_u/s_{ur}) was either reported or inferred from laboratory test results by Brand et al. (1972), Jardine et al. (1995), and Stuedlein and Holtz (2010). For the remaining portion of the database, s_{ur} was estimated based on a correlation to the liquidity index, LI, following Najjar (2005), based on Wroth and Wood (1978):

$$s_{ur}=170e^{-(4.6LI)} \quad (11)$$

where s_{ur} is in kPa. Najjar (2005) suggests the correlation is appropriate for soils with a sensitivity in the range of 2 to 5. Therefore, where Eq. (11) predicted residual soil shear strengths with corresponding sensitivity falling outside of a range of 2 to 5, the assumed residual shear strength was revised to limit the minimum sensitivity value equal to 2 and maximum value equal to 5. Note, application of the reliability-based SLS design procedures described subsequently is not recommended for use with extremely sensitive soils (i.e., soils with sensitivity greater than five).

The ratio of bearing capacity calculated using s_{ur} (i.e., the lower-bound capacity) to those calculated using s_u was computed and produced a mean lower-bound bearing capacity

ratio of 0.47 and standard deviation of 0.18. Therefore, a normalized bearing capacity, $q^*_{ult,\ min}$, of 0.29, representing the mean ratio minus one standard deviation, was selected to truncate the q^*_{ult} distribution in the MCS. The inclusion of the lower-bound capacity reduced the number of simulations by approximately 0.1 percent; although not representing a large number of simulations, inclusion of the truncated capacity distribution improves the accuracy of reliability calibrations and removes unnecessary conservatism.

9. Characterization of applied bearing pressure

The load and resistance factor calibrated herein for SLS design considered uncertainty in the applied bearing pressure in order to maintain consistency with widely-accepted loading scenarios. The loading was modeled using a unit mean normalized applied bearing pressure, q^*_{app}, equal to 1.00 and COV(q^*_{app}) equal to 10 and 20 percent for dead and live loads, respectively (Table 6). These values suggest that, on average, structure loads can be estimated with relatively close accuracy, but the design accounts for some potential deviation. The unit mean normalized applied bearing pressure was modeled using a lognormal distribution, consistent with national codes (e.g., AASHTO, 2012) and reliability analyses performed by others (e.g., Phoon and Kulhawy, 2008; Uzielli and Mayne, 2011; Li et al., 2013).

10. Characterization of allowable displacement

Considering the end-user of a calibrated SLS design procedure, an appropriate load and resistance factor should be selected based on a structures' ability to accept deformations arising from foundation movements. This is a function of the structure type and its intended use, and requires close collaboration with the entire design team. To provide a generalized framework, this study explicitly incorporated a continuous range in the allowable immediate displacements, δ_a, in the estimate of the mobilized resistance using the relevant performance function (Eq. (7)). Table 7 summarizes the selected normalized allowable displacements, η_a, which ranged from 0.005 to 0.20, based on an assumed range of mean δ_a of 2.5 mm to 600 mm and equivalent footing diameters, B', ranging from 0.5 m to 3 m. The dispersion in B' was modeled using a COV of 2 percent and a normal distribution. It should be noted that the upper values of δ_a were included to provide the selected range of η, and δ_a may approach unrealistic magnitudes as a result.

Unlike the selection of a representative magnitude of uncertainty in loading, there is not yet a consensus on the suitable design-level dispersion in the allowable immediate or total displacement largely owing to the lack of available data. Phoon and Kulhawy (2008) assumed a COV of 60 percent for δ_a based on research by Zhang and Ng (2005) for structures supported on deep foundations. However, they concede that it is unclear whether available data for allowable displacement typically refers to mean or lower-bound values, which may also affect its dispersion. Uzielli and Mayne (2011) assumed a COV of 60 percent for δ_a and lognormal distribution when analyzing the SLS for spread footings on sand. For this study, δ_a was modeled using a lognormal distribution and COV of 0, 20, 40 and 60 percent to represent a range of COV, in order to allow professional judgment in the selection of the appropriate lumped load and resistance factor for the corresponding COV(δ_a).

11. Reliability simulations and lumped factor calibration

Monte Carlo simulations were used to generate samples from each of the random variable distributions as a means to populate the performance function (Eq. (7)) and calibrate the lumped load and resistance factor, ψ_q, to the probability of exceeding the SLS (and corresponding β value). Each random variable (i.e., k_1, k_2, M_{STC}, δ_a, B', q^*_{ult} and q^*_{app}) was randomly sampled using their source distribution and 1.5×10^6 simulations for each ψ_q, which ranged from 1 to 20. The final number of simulations (i.e., the basis for computing p_f and β) was slightly smaller than 1.5×10^6, as simulations associated with $q^*_{ult,min}$ less than 0.29 were rejected to enforce the truncated bearing capacity distribution as described previously. The reliability calibrations required approximately 2500 independent simulation scenarios in order to estimate β and p_f for different combinations of ψ_q, B', δ_a, COV(δ_a), and COV(q^*_{app}), and are associated with a confidence level of 99 percent or greater for simulations corresponding to β less than or equal to four, sufficiently accurate for reliability levels corresponding to the SLS.

The results of the simulations indicated strong non-linear relationships between ψ_q and β at any given η_a. Consistent with the service limit displacements of footings on sand reported by Uzielli and Mayne (2011, 2012) and on aggregate pier reinforced clay (Huffman and Stuedlein, 2014), the relationships of β and ψ_q were nearly identical regardless of the δ_a and B' values used to define η_a. Fig. 5 shows the ψ_q calibration for

Table 7
Summary of assumed normalized bearing pressure and displacement parameters

Parameter	Nominal value	COV (%)	Model distribution
q^*_{app}	1.00	10, 20	Lognormal
δ_a (mm)	2.5, 5, 7.5, 10, 12.5, 15, 20, 25, 30, 37.5, 50, 75, 100, 112.5, 125, 150, 187.5, 200, 225, 250, 300, 400, 500, 600	0, 20, 40, 60	Lognormal
B' (m)	0.5, 1.0, 1.5, 2.0, 2.5, 3.0	2	Normal
η	0.005, 0.01, 0.025, 0.05, 0.075, 0.10, 0.20	–	–

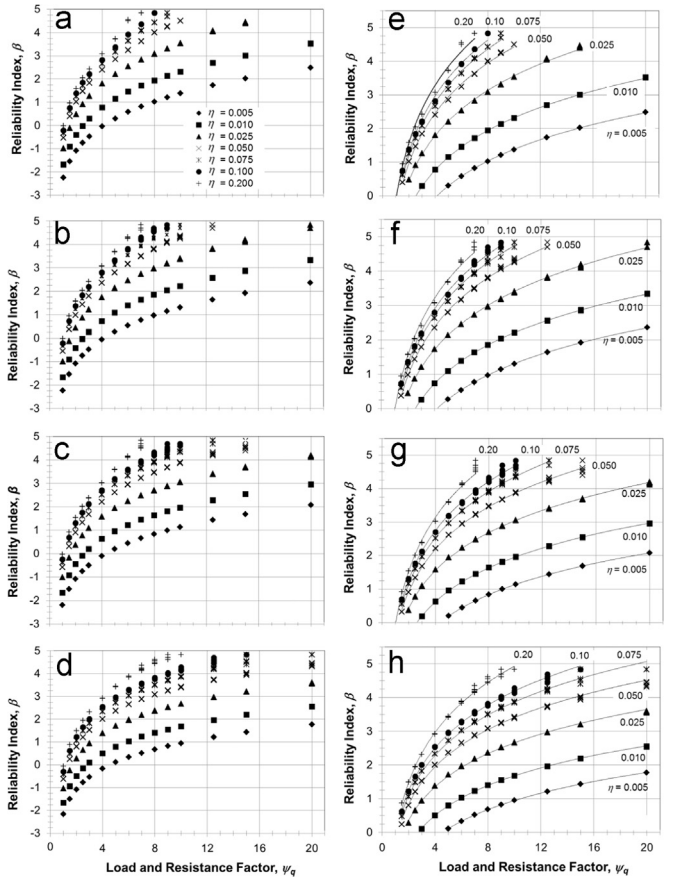

Fig. 5. Load and resistance factor, ψ_q, and reliability index, β, varying with normalized displacement, η, for COV(q_{app})=0.10 and (a and e) COV(δ_a)=0, (b and f) COV(δ_a)=20 percent, (c and g) COV(δ_a)=40 percent, and (d and h) COV(δ_a)=60 percent. Note, logarithmic-fitted curves shown in (e) through (h) are limited to $\beta > 0$.

COV(q^*_{app}) of 10 percent, and COV(δ_a) ranging from 0 to 60 percent from the MCS. Fig. 5(a) through (d) includes the results of the entire simulation, whereas Fig. 5(e) through (h) includes only β values greater than 0, in order to improve the fit of logarithmic trendlines over ψ_q–β pairs that may be suitable for design.

The MCS showed that low reliability indices (i.e., high probability of exceeding the selected magnitude of displacement) logically correspond to low values of ψ_q. Further, the reliability indices increased sharply with moderate increases in ψ_q. For example, considering an unfactored loading case (i.e., ψ_q=1.0) in Fig. 5(a), at a normalized allowable immediate displacement, η_a, of 0.025, β is equal to −0.98, which corresponds to a probability of exceeding η_a of approximately 84 percent. At the same η_a, but considering ψ_q equal to 3, β rises to 1.26 and a corresponding 10 percent probability of exceeding η_a. As shown in Fig. 5, similar trends in the variation of ψ_q with β were noted for the reliability simulations corresponding to the range in COV(q^*_{app}) and COV(δ_a) investigated.

Uzielli and Mayne (2011) suggested the ψ_q vs. β relationship could be characterized with the functional form:

$$\beta = p_1\, ln(\psi_q) + p_2 \tag{12}$$

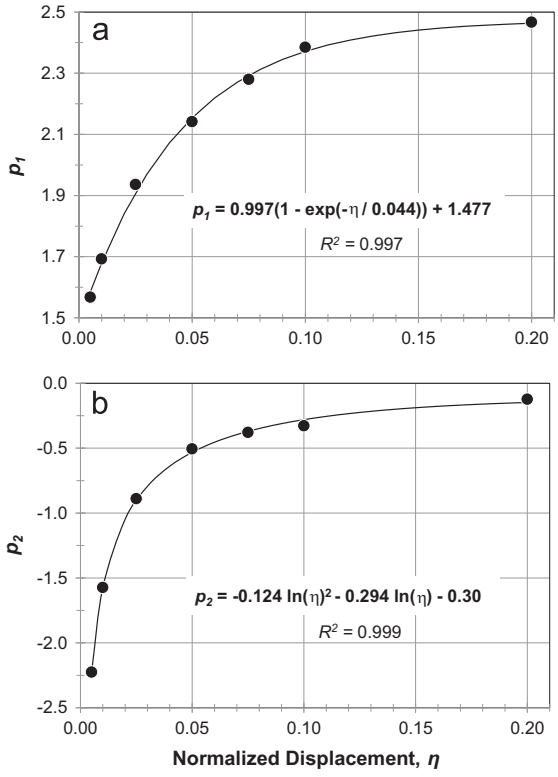

Fig. 6. Variation of regressed coefficients (a) p_1 and (b) p_2 with normalized displacement. Curves shown for COV(q_{app})=10 percent and COV(δ_a)=0.

for their reliability simulations, where p_1 and p_2 are best fit coefficients. Uzielli and Mayne (2011) also found the coefficient p_1 and constant p_2 varied with the normalized allowable displacement, η_a, in a linear and logarithmic trend, respectively. For this study, p_1 was found to correlate with a three-parameter exponential function of the form:

$$p_1 = a\left(1 - exp\left(-\eta_a/b\right)\right) + c \tag{13}$$

and p_2 was found to correlate well with a three-parameter log-polynomial function:

$$p_2 = d\,\ln(\eta) + e\,\ln(\eta) + f \tag{14}$$

where a, b and c in Eq. (13) and d, e and f in Eq. (14) are estimated using least squares optimization. Fig. 6 shows an example of the regressed, best-fit curves for p_1 and p_2 for the case of COV(q^*_{app})=10 percent and COV(δ_a)=0. Combining the models used to predict p_1 and p_2 with Eq. (12) yields the closed-form model to estimate the reliability index:

$$\beta = \left(a\left(1 - \exp\left(\frac{-\eta_a}{b}\right)\right) + c\right)\ln\left(\psi_q\right) + d\,\ln\left(\eta_a\right)^2 + e\,ln(\eta) + f \tag{15}$$

which is associated with a confidence level of 99 percent or better for $\beta < 4$. Table 8 provides a summary of the best-fit coefficients a, b, c, d, e and f to estimate the reliability index associated with any η_a and ψ_q for Eq. (15). Note the coefficients will vary depending on the anticipated dispersion of the allowable immediate footing settlement and applied bearing pressure. Alternatively, the load and resistance factor associated with any β and η_a may be computed by inverting

Table 8
Summary of best-fit coeff. for Eqs. (15) and (16) and multiplying factor, $M_{\psi,95}$.

COV (δ_a) (%)	COV (q^*_{app}) (%)	a	b	c	d	e	f	$M_{\psi,95}$
0	10	0.997	0.044	1.477	−0.124	−0.294	−0.300	1.08
20	10	0.974	0.045	1.412	−0.121	−0.285	−0.245	1.06
40	10	1.099	0.073	1.299	−0.136	−0.429	−0.444	1.05
60	10	1.164	0.114	1.176	−0.103	−0.181	0.096	1.09
0	20	0.733	0.033	1.417	−0.122	−0.277	−0.159	1.05
20	20	0.778	0.037	1.359	−0.116	−0.252	−0.126	1.06
40	20	0.869	0.063	1.273	−0.128	−0.369	−0.278	1.05
60	20	1.049	0.114	1.163	−0.096	−0.135	0.193	1.10

Eq. (15):

$$\psi_q = \exp\left[\frac{\beta - d\ln\left(\eta_a\right)^2 - e\ln\left(\eta_a\right) - f}{a\left(1-\exp\left(\frac{-\eta_a}{b}\right)\right)+c}\right] \tag{16}$$

such that the required load and resistance factor can be obtained for a desired level of reliability.

12. Comparison of MCS results and closed-form model

The closed-form model used to predict the load and resistance factor for the given normalized displacement and reliability index introduces variability owing to the errors associated with the fitting to the reliability simulations (i.e., Eqs. (12)–(14)). To quantify the error, the β values produced by the fitting to the MCS were substituted into Eq. (16) to calculate ψ_q and compare to the actual MCS. The results of the comparison are plotted in Fig. 7 for the range of COV(q^*_{app}) and the range of COV(δ_a) investigated and for β resulting from the prescribed interval of ψ_q ranging from 1 to 20. A mean bias of 1.0 was calculated for each combination of COV(q^*_{app}) and COV(δ_a), with COV in the bias ranging from 2.2 to 5 percent, indicating relatively small error. The error typically becomes greater at the largest values of ψ_q, which is attributed primarily to the larger dispersion of p_f and β estimated from the MCS for large ψ_q values (Fig. 5) and error in the hyperbolic q^*–η model at small displacements.

To account for the error in Eq. (16) and the increased dispersion at the largest values of ψ_q, a factor $M_{\psi,95}$ may be multiplied by ψ_q such that a lumped load and resistance factor, $\psi_{q,95} = \psi_q * M_{\psi,95}$ represents the 95 percent confidence level in the simulation-based ψ_q. Adjustment factors ranging from $M_{\psi,95}$ = 1.05 to 1.10 were computed for the various combinations of COV (q^*_{app}) and COV(δ_a), and are provided in Table 8.

13. Application of the reliability calibrations

13.1. Design example

Upon loading, a spread footing on clay will experience immediate displacement in addition to consolidation settlement and possibly secondary compression. Therefore, the foundation designer will need to establish the total tolerable displacement, and then perform the required analyses to determine whether one component of displacement or a combination of these components is likely to exceed the target probability associated with exceeding the tolerable displacement. Settlement analysis associated with consolidation is well established and not addressed herein. Instead the focus is on immediate displacement only. The following steps (Fig. 8) are required to estimate the corresponding allowable bearing pressure associated with a 1 percent probability of exceedance (β=2.33) for a typical equivalent footing diameter of 1 m and nominal allowable immediate footing displacement of 25 mm:

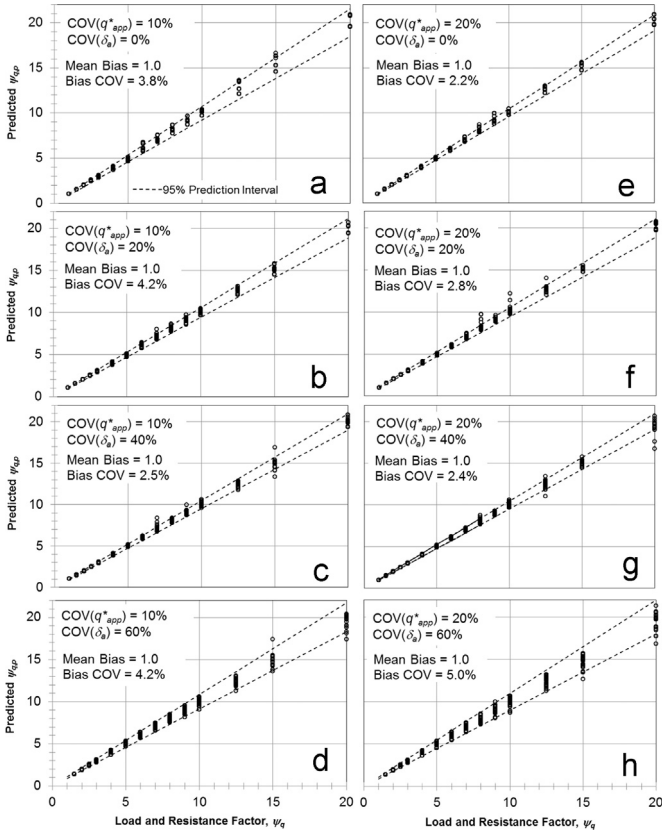

Fig. 7. Comparison of MCS-based load and resistance factor, ψ_q and predicted load and resistance factor, $\psi_{q,p}$ using Eq. (16), along with 95 percent prediction interval. Comparisons in (*a*) through (*d*) represent COV(q^*_{app})=10 percent, whereas comparisons in (*e*) through (*h*) represent COV(q^*_{app})=20 percent.

1. Estimate the bearing capacity of the spread footing using Eq. (1). That is, calculate $q_{ult,p}$.
2. Establish the mobilized resistance, q_{mob}, using Eq. (4) with the allowable immediate displacement and estimated slope tangent capacity, q_{STC}. For this example, the normalized allowable immediate displacement, η_a, is 0.025. The coefficients k_1 and k_2 provided in Table 5 are 0.013 and 0.701, respectively, resulting in a hyperbolic model factor, M_η, of 0.819. The slope tangent model factor, M_{STC}, is 0.643 (Table 5). Therefore, the mobilized resistance is $(0.819)(0.643)q_{ult,p} = 0.527q_{ult,p}$.
3. The resistance factor, ψ_q, is applied to $q_{ult,p}$ based on the

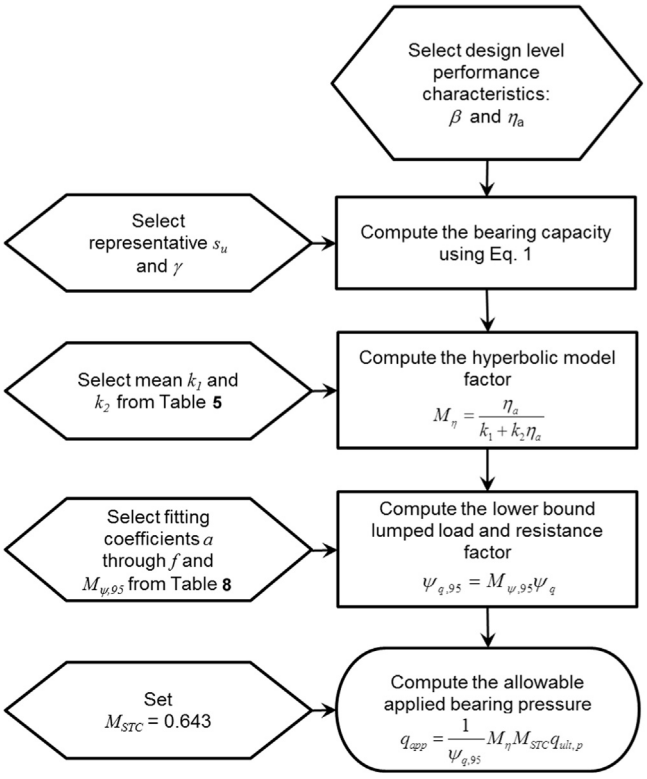

Fig. 8. Procedure for implementation of the proposed reliability-based serviceability limit state methodology for immediate settlements of spread footings on plastic, fine-grained soils.

selected target probability of exceeding the service level displacement. Estimate ψ_q using Eq. (16) based on the allowable immediate displacement and coefficients *a, b, c, d, e and f* (Table 8). A COV(δ_a) and COV(q^*_{app}) of 0 and 10 percent were assumed, respectively, for this example. For a p_f of 1 percent ($\beta=2.33$), ψ_q equals approximately 5.4 using Eq. (16). The adjustment factor, $M_{\psi,95}=1.08$ (Table 8) is recommended for the prescribed COV(δ_a) and COV(q^*_{app}) values, resulting in a $\psi_{q,95}$ value of approximately 5.8.

4. The allowable bearing pressure that limits immediate displacement to 25 mm or less with probability of exceeding the allowable immediate displacement of 1 percent may then be computed by combining the results from steps 1 through 3, resulting in $(1/\psi_{q,95})(M_\eta)(M_{STC})(q_{ult,p})$, or $0.09q_{ult,p}$.

14. Discussion

An interesting result of the example provided above is to note that the selected probability of 1 percent of exceeding the immediate displacement produced a relatively low bearing pressure value (i.e., $0.09q_{ult}$). Allowable stress design (ASD) factors of safety for spread footings typically range between 3 to 4 (i.e., $0.25q_{ult}$ to $0.33q_{ult}$). For the design example included above, this range of ASD factors of safety results in an equivalent ψ_q factor ranging from 1.32 to 1.57, and a probability of exceeding the allowable immediate displacement ranging from 50 to 64 percent. This suggests that evaluating a spread footing on clay using traditional formulas to determine bearing capacity (i.e., ULS) and applying a typical ASD factor of safety in the range of 3 to 4 could result in a relatively high probability of exceeding the target immediate displacement. On the other hand, Eurocode 7 (e.g., Orr and Breysse, 2008) includes SLS provisions of $\beta=1.5$ (or $p_f=6.7$ percent) over a 50 year service life. For these less stringent conditions, $\psi_{q,95}=3.80$ and $q=0.14q_{ult,p}$, representing an increase in bearing pressure of more than 50 percent. Thus, the designer's judgment can be readily incorporated into the proposed RBD procedure based on the quality of information and the requirements of the structure. Note that for the given examples, where $\delta_a=25$ mm, the margin of immediate displacement exceeding the target magnitude could range from an insignificant amount (i.e., on the order of 1 mm) or a significant amount (10 mm). Obviously, efforts to improve the understanding of the spatial variability of pertinent design parameters at a particular site to reduce the overall risk of exceeding a given limit state remain warranted.

Immediate displacement may comprise just a portion of the total settlement under a given foundation and separate analyses must be conducted to estimate consolidation settlements if the possibility for triggering primary consolidation exists. Additionally, the practitioner must estimate the total differential settlement possible, and the procedure proposed herein can be used to help judge the likelihood of exceeding a target immediate differential settlement. This can be useful where staged construction is required, or where footings of significantly different bearing pressures or bearing loads are to be supported. In practice, when the duration between successive construction loads is long, and where strength gain occurs, the procedure described herein may be updated to reflect the increased capacity and refine the estimate of immediate and differential settlement. Additionally, it is recommended that practitioners perform separate analyses for the assessment of construction, using dead loads and dead load statistics, and for live loading events that may occur over the life of the structure. The gain in strength resulting from possible consolidation should be incorporated into the evaluation of immediate settlement for long-term live loading events. Finally, when justified, the procedure described herein can be used to plan and execute footing loading tests conducted to support design recommendations.

15. Summary

This paper describes the development of a reliability-based SLS procedure for the estimation of the allowable bearing pressure at a given immediate displacement and its corresponding probability of exceeding this value for spread footings on plastic, fine-grained soils. The framework developed herein was based on a new loading test database to characterize and simulate the nonlinear, inelastic bearing pressure–displacement response. First, the normalized bearing pressure–displacement (q^*–η) response was estimated based on a novel reference slope-tangent capacity and hyperbolic resistance-mobilized displacement model. The probability of exceeding the estimated immediate displacement was then established using a performance function and Monte Carlo simulations in combination with the dispersion of the

various controlling loading and resistance parameters. Correlation in the resistance parameters was accounted for using appropriate vine copulas, and truncation of the lower-bound resistance was accomplished using methods proposed by Najjar and Gilbert (2009).

Evaluation of the Monte Carlo simulations indicated a nonlinear relationship between the load and resistance factor, ψ_q, and the reliability index, β, used to reference a target probability of exceeding the SLS design. A new and convenient set of equations were proposed to provide ψ_q given a target β value based on an acceptable probability of exceeding the allowable immediate displacement. In order to illustrate the use of the proposed procedure, an example of its application was provided. The results of the example suggested that the probability of exceeding the allowable immediate settlement can be relatively high using traditional factors of safety, although the magnitude of the settlement exceeding SLS may range from insignificant to significant.

The analysis and procedure presented herein is appropriate for estimating immediate undrained settlement of rigid footings on plastic fine-grained soil with undrained shear strengths in the relative range of soft to stiff, and for evaluating the reliability of the settlement calculation. Because the spatial variability and measurement errors were not explicitly treated in this study, the results of this study should not be extrapolated to foundation or soil conditions that are outside the range included in the database.

References

Aas, K., Czado, C., Frigessi, A., Bakken, H., 2009. Pair-Copula construction of multiple dependence. Insur.: Math. Econ. 44 (2), 182–198.

AASHTO , 2012. AASHTO LRFD Bridge Design Specifications, sixth ed. AASHTO, Washington, DC.

Akaike, H., 1974. A new look at the statistical model identification. IEEE Trans. Autom. Control 19 (6), 716–723.

Akbas, S.O., Kulhawy, F.H., 2009. Axial compression of footings in cohesionless soils. I: Load–settlement behavior. J. Geotech. Geoenviron. Eng. ASCE 135 (11), 1562–1574.

Allen, T.A., Nowak, A.S., Bathurst, R.J., 2005. Calibration to Determine Load and Resistance Factors for Geotechnical and Structural Design Transportation Research Circular E-C079. Transportation Research Board of the National Academies, Washington, DC, 93.

Andersen, K.H., Stenhamar, P., 1982. Static plate loading test on overconsolidated clay. J. Geotech. Eng. Div. ASCE 108 (7), 918–934.

Baecher, G.B., Christian, J.T., 2003. Reliability and Statistics in Geotechnical Engineering. John Wiley and Sons, Ltd, London and New York, 605.

Bauer, G.E., Shields, D.H., Scott, J.D., 1976. Predicted and Observed Footing Settlements in a Fissured Clay. Pentech Press, Ottawa287–302.

Bergado, D.T., Rantucci, G., Widodo, S., 1984. Full scale load tests of granular piles and sand drains in the soft Bangkok clay. Asian Inst. Technol., 111–118.

Brand, E.W., Muktabhant, C., Taechathummarak, A., 1972. Load tests on small foundations in soft clay. In: Conference Proceedings: Performance of Earth and Earth Supported Structures, ASCE, pp. 903-928.

Brechmann, E.C., Schepsmeier, U., 2013. Modeling dependence with C- and D-vine copulas: the R package CDVine. J. Stat. Softw. 52 (3), 27.

Consoli, N.C., Schnaid, F., Milititsky, J., 1998. Interpretation of plate load tests on residual soil site. J. Geotech. Geoenviron. Eng. ASCE 124 (9), 857–867.

D'Appolonia, Lambe, T.W., 1970. Method for predicting initial settlement. J. Soil Mech. Found. Div. ASCE 96 (SM2), 523–544.

D'Appolonia, D., Poulos, H., Ladd, C., 1971. Initial settlement of structures on clay. J. Soil Mech. Found. Div. 97 (SM10), 1359–1377.

Deshmukh, A.M., Ganpule, V.T., 1994. Influence of flexible mat on settlements of marine clay. In: Vertical and Horizontal Deformations of Foundations and Embankments, ASCE, pp. 887-896.

Fenton, G.A., Griffiths, D.V., Cavers, W., 2005. Resistance factors for settlement design. Can. Geotech. J. 42 (5), 1422–1436.

Foye, K.C., Basu, P., Prezzi, M., 2008. Immediate settlement of shallow foundations bearing on clay. Int. J. Geomech. ASCE 8 (5), 300–310.

Greenwood, D.A., 1975. Vibroflotation: rationale for design and practice. In: Bell, F.G. (Ed.), Methods of Treatment of Unstable Ground. Newness-Buttersworth, London, UK, pp. 189–209.

Hansen, J.B., 1970. A revised and extended formula for bearing capacity. DGI Bull., 5–11.

Huffman, J.C., Stuedlein, A.W., 2014. Reliability-based serviceability limit state design of spread footings on aggregate pier reinforced clay. J. Geotech. Geoenviron. Eng. ASCE 140 (10), 04014055.

Jardine, R.J., Lehane, B.M., Smith, P.R., Gildea, P.A., 1995. Vertical loading experiments on rigid pad foundations at bothkennar. Geotechnique 45 (4), 573–597.

Jardine, R.J., Potts, D.M., Fourie, A.B., Burland, J.B., 1986. Studies of the influence of non-linear stress–strain characteristics in soil–structure interaction. Geotechnique 36 (3), 377–396.

Joe, H., 1996. Families of m-variate distributions with given margins and $m(m-1)/2$ bivariate dependence parameters, Distributions with Fixed Marginals and Related Topics. Institute of Mathematical Statistics120–141.

Lambe, T.W., Whitman, R.V., 1969. Soil Mechanics. John Wiley and Sons, Inc., New York, NY.

Lehane, B.M., 2003. Vertically loaded shallow foundation on soft clayey silt. ICE Geotech. Eng. 156 (1), 17–26.

Li, D.Q., Tang, X.S., Phoon, K.K., Chen, Y.F., Zhou, C.B., 2013. Bivariate simulation using Copula and its application to probabilistic pile settlement analysis. Int. J. Numer. Anal. Methods Geomech. 37 (6), 597–617.

Lipster, R.S., Shiryaev, A.N., 2001. Statistics of Random Processes II: Applications, second ed Springer-Verlag, Berlin.

Marsland, A., Powell, J.J.M., 1980. Cyclic Loading Tests on 865 mm Diameter Plates of a Stiff Clay Till. Balkema Press, Swansea837–847.

Meyerhof, G.G., 1963. Some recent research on the bearing capacity of foundations. Can. Geotech. J. 1 (1), 16–26.

Mayne, P.W., Poulos, H., 1999. Approximate displacement influence factors for Elastic Shallow Foundations. Journal of Geotechnical and Geoenvironmental Engineering 125 (6), 453–460.

Najjar, S.S., 2005. The Importance of Lower-Bound Capacities in Geotechnical Reliability Assessments. University of Texas at Austin, 317 Ph.D. Thesis.

Najjar, S.S., Gilbert, R.B., 2009. Importance of lower-bound capacities in the design of deep foundations. J. Geotech. Geoenviron. Eng. ASCE 135 (7), 890–900.

Nelson, R.B., 2006. An Introduction to Copulas, 2nd Ed. Springer, New York 269 p..

Newton, V.C., 1975. Ultimate Bearing Capacity of Shallow Footings on Plastic Silt. Oregon State University, 49 M.S. Thesis.

Orr, T.L., Breysse, D., 2008. Eurocode 7 and reliability-based design. In: Phoon, K.K. (Ed.), Reliability-based Design in Geotechnical Engineering: Computations and Applications. Taylor and Francis, pp. 298–343 Chapter 8.

Phoon, K.K., 2003. Practical guidelines for reliability-based design calibration. Paper presented at session TC 23 (1) advances in geotechnical limit state design. In: Twelfth Asian Regional Conference on SMGE, August 7–8, 2003, Singapore.

Phoon, K.K., 2008. Numerical recipes for reliability analysis—a primer, Reliability-Based Design in Geotechnical Engineering: Computations and Applications. Taylor and Francis, London1–75.

Phoon, K.K., Kulhawy, F.H., 2008. Serviceability limit state reliability-based design, Reliability-Based Design in Geotechnical Engineering: Computations and Applications. Taylor and Francis, London344–384.

Roberts, L.A., Misra, A., 2010. LRFD of shallow foundations at the service limit state : Assessment and Management of Risk for Engineered Systems and Geohazards. Georisk 4 (1), 13–21.

Strahler, A.W., 2012. Bearing Capacity and Immediate Settlement of Shallow Foundation on Clay. Oregon State University, 214 M.S. Thesis.

Strahler, A.W., Stuedlein, A.W., 2013. Characterization of model uncertainty in immediate settlement calculations for spread footings on clay. In: Proceedings of 18th International Conference on Soil Mechanics and Geotechnical Engineering, Paris, 2014, 4 p.

Strahler, A.W., Stuedlein, A.W., 2014. Accuracy, uncertainty, and reliability of the bearing capacity equation for shallow foundations on saturated clay In: Geo-Characterization and Modeling for Sustainability, GeoCongress 2014, GSP No. TBD, ASCE, Atlanta, GA, February 23–26, 2014, 12 p.

Stuedlein, A.W., Holtz, R.D., 2010. Undrained displacement behavior of spread footings in clay. In: Honoring Clyde, N., Baker Jr., P.E., S.E. (Eds.), The Art of Foundation Engineering Practice. ASCE, pp. 653–669.

Stuedlein, A.W., Reddy, S.C., 2013. Factors affecting the reliability of augered cast-in-place piles in granular soils at the serviceability limit state. J. Deep Found. Inst. 7 (2), 46–57.

Stuedlein, A.W., Uzielli, M., 2014. Serviceability limit state design for uplift of helical anchors in clay. Geomech. Geoeng. 9 (3), 173–186.

Stuedlein, A.W., Neely, W., Gurtowski, T., 2012. Reliability-based design of augered cast-in-place piles in granular soils. J. Geotech. Geoenviron. Eng. ASCE 138 (6), 709–717.

Schwarz, G., 1978. Estimating the dimension of a model. Ann. Stat. 6 (2), 461–464.

Tand, K.E., Funegard, E.G., Briaud, J.L., 1986. Bearing capacity of footings on clay CPT method. In: Use of In Situ Tests in Geotechnical Engineering, ASCE, pp. 1017-1033.

Tang, X.S., Li, D.Q., Rong, G., Phoon, K.K., Zhou, C.B., 2013. Impact of copula selection on geotechnical reliability under incomplete probability information. Comput. Geotech. 49, 264–278.

Tang, X.S., Li, D.Q., Zhou, C.B., Phoon, K.K., Zhou, C.B., 2015. Copulas-based approaches for evaluating slope reliabiilty under incomplete probability information. Struct. Saf. 50, 90–99.

Terzaghi, K., 1943. Theoretical Soil Mechanics. John Wiley and Sons, Inc, New York, NY.

Uzielli, M., Mayne, P., 2011. Serviceability limit state CPT-based design for vertically loaded shallow footings on sand : An International Journal. Geomech. Geoeng. 6 (2), 91–107.

Uzielli, M., Mayne, P., 2012. Load–displacement uncertainty of vertically loaded shallow footings on sands and effects on probabilistic settlement. Georisk 6 (1), 50–69.

Vesic, A.S., 1973. Analysis of Ultimate Loads of Shallow Foundations. Journal of the Soil Mechanics and Foundations Division, American Society of Civil Engineers 99 (SM1), 45–73.

Wang, Y., 2011. Reliability-based design of spread foundations by Monte Carlo simulations. Geotechnique 61 (8), 677–685.

Wroth, C.P., Wood, D.M., 1978. The correlation of index properties with some basic engineering properties of soils. Can. Geotech. J. 15 (2), 137–145.

Wu, X.Z., 2013. Trivariate analysis of soil ranking-correlated characteristics and its application to probabilistic stability assessments in geotechnical engineering problems. Soils Found. 53 (4), 540–556.

Wu, X.Z., 2015. Assessing the correlation performance functions of an engineering system via probabilistic analysis. Struct. Saf. 52, 10–19.

Zhang, L.M., Ng, A.M.Y, 2005. Probabilistic limiting tolerable displacements for serviceability limit state design of foundations. Geotechnique 55 (2), 151–161.